HHS Public Access

Author manuscript

Exp Eye Res. Author manuscript; available in PMC 2022 June 13.

Published in final edited form as:

Exp Eye Res. 2021 April ; 205: 108444. doi:10.1016/j.exer.2021.108444.

Layer-specific nanophotonic delivery of therapeutic opsin-encoding genes into retina

Subrata Batabyal, **Sanghoon Kim**, **Weldon Wright**, **Samarendra Mohanty***

Nanoscope Technologies LLC, 1312 Brown Trail, Bedford, Texas, USA, 76022

Abstract

In recent time, gene therapy has proven to be a promising remedial approach for treating visual disorders either by replacement of nonfunctioning gene(s) or by introduction of light sensitive proteins (opsins) as artificial photoreceptors in retinal cells. Conventional viral vector-based gene delivery method is often confronted with limitations due to immunogenetic reaction, unintended non-targeted delivery, non-feasibility of repeated re-dosing due to immunorejection, and complicated manufacturing process, leading to significant roadblock in translational success. In this regard, non-viral delivery provides a safer, simpler and cost-effective alternative. However, most of the non-viral approaches lack spatial and/or cellular specificity and limited by low transfection efficacy and cytotoxicity. Here, we present a minimally invasive, non-viral and clinically translatable safe targeted gene delivery method utilizing functionalized plasmonic gold nanorods (fGNRs, targeted to attach to specific cell types of the organ of interest) and spatially targeted controlled light irradiation. Targeted in-vivo delivery and expression of opsin-encoding gene in bipolar and ganglion cell layers were achieved by use of cell specific fGNRs concurrent with light irradiation. Evaluation of safety and toxicity associated with the transduction of opsin-encoding genes by use of fGNRs and light irradiation were examined by electrophysiology, Optical coherence tomography, intra-ocular pressure and other analytical methods (confocal microscopy, immunohistochemistry). The non-viral light-based opsin-gene delivery provides a safe and effective alternative to viral-vector based gene delivery and holds promise for corrective cell-specific gene therapies for retinal degenerative diseases.

Keywords

Non-viral delivery; Retinal gene therapy; Photoreceptor degeneration; Optogenetics

*Corresponding Author: smohanty@nanoscopetech.com.

Author Contributions

SB prepared the plasmids and fGNRs. SB, SK and SM carried out the optical delivery experiments. SB performed immunohistochemistry. SB and SM performed confocal microscopy imaging and SK performed the OCT imaging. SB, SK and SM and carried out the data analysis. SB and SM performed the ERG and IOP measurements. WW provided inputs and participated in discussion. SM designed the experiments and supervised the project. The manuscript was written through contributions of all authors.

Competing financial interests

The author Samarendra Mohanty has equity interest in Nanoscope Technologies LLC.

Introduction

The introduction of foreign DNA[1], short-interfering RNA[2], CRISPR/Cas9, small molecules, proteins[3] and drugs into living cells, organs and whole organisms is essential for a variety of applications in genetics, cell and developmental biology, vaccination[4], gene therapy[5,6] and other therapeutic strategies. Efficient and safe gene delivery to targeted cell types is the fundamental requirement for a successful gene therapy program. Though the viral based transduction has been the go-to delivery method for most of the current gene therapy trial due to its relatively high transfection efficacy, it is not the ideal as it has several drawbacks such as immunogenicity and cytotoxicity. In fact, the first related fatality of gene therapy clinical trial was related to the inflammatory reaction to the viral vector (Adenovirus). Further adeno-associated virus and lentiviruses have limitation in packaging capacity with carrying size DNA within 5-10 Kb[7,8]. Viral delivery arose from removal of pathogenic viral DNA sequences from viruses by researchers, while preserving the virus' ability to infect and transfer genetic material into cells, a process called gene transduction. This has been done with many viruses, including retrovirus[9], adenovirus[10], herpes simplex virus (HSV), AAV[11], and pox virus[12]. All of these have attractive features, particularly their high gene transduction capability. However, no matter how attenuated these viral particles are, there are still biosafety concerns, especially innate and immune barriers[13], toxicity[14], and potential recombination of or complementation *in vivo* which can generate virulent viral pathogens after vector delivery[15]. The size of viral vectors, which restricts the size of the genetic materials that can be administered, is another limitation[16]. Use of non-viral physical[17,18] and chemical[19] methods have gain popularity in last decade due to their low immunotoxicity, ease of production and safety. Significant progress have been made for development of non-viral gene delivery method, including physical (microinjection[20], gene gun, electroporation[18,21], ultrasound[17], hydrodynamic, magnetofection) and chemical (liposomes[19], biodegradable polymer nanoparticles[22]) methods. Non-viral gene delivery approaches have advantage of sustained tunable gene expression suitable for the stage of the disease[23]. However, most of the available non-viral methods often cases lack specificity, site selectivity and inherently have low transient transfectability.

For gene therapy, eye is an excellent target because it is easily accessible for gene delivery and immune-privileged[24]. However, proper control of gene expression is required in terms of level of the gene product and cell/tissue specific expression[25]. Clinical translation of cell gene therapy for treatment of retinal dystrophy requires spatial targeted delivery of therapeutics molecules into specific cell type without perturbing the functional region of retina[26]. This necessitates development of non-viral method for gene delivery to spatially targeted region(s) of retina in a minimally invasive manner. Recently, opto-gene[27] therapies based on precise optical modulation[28–31] of nervous system is receiving significant attention for treatment of several neurological and retinal disorders [32–38]. Opto-gene therapies of retinal degenerative diseases such as dry age-related macular degeneration (dry-AMD) require photosensitization of higher order retinal neurons[39,40,41]. However, most of the non-viral delivery methods have reduced transfection efficiency as well as adverse effects on non-targeted cells[18]. Furthermore, irrespective of the viral or non-viral method used for gene delivery, it is difficult to spatially control the region of gene expression in the

organ of interest. Therefore, new strategies are needed to achieve safe, efficient and targeted gene delivery. Recently, we demonstrated a minimally invasive, non-viral targeted laser-based gene delivery method[42,43] utilizing functionalized plasmonic gold nanorods (fGNRs). However, Concanavalin-A was used for non-specific binding of fGNRs to the cells in proximity of the delivery site (i.e., Ganglion cell layer) upon intravitreal injection.

Here, we present use of cell-specific functionalization of two different GNRs having different surface plasmon resonance (SPR) peaks so as to bind to different cell types of retina and activate targeted gene delivery by spatially targeted controlled irradiation of near-infrared light with wavelength tuned to the SPR peak. Targeted in-vivo delivery and expression of opsin-encoding gene in bipolar and ganglion cell layers were achieved by use of PKCα and Thy1 functionalized GNRs followed by light irradiation. Evaluation of safety and toxicity associated with the transduction of opsin-encoding genes by use of fGNRs and light irradiation was examined by optical coherence tomography, intra-ocular pressure, electroretinogram, and other analytical methods including quantitative PCR, confocal microscopy, and immunohistochemistry. The non-viral light-based opsin-gene delivery to targeted retinal layers provides an efficient alternative to viral-vector based gene delivery and the method provides a potential means for corrective cell-specific gene therapies for retinal degenerative diseases.

Results

Principle of layer-specific optical delivery of opsin-encoding genes by use of cell-specific functionalized gold nanorods

The biggest impediment to delivering impermeable exogenous therapeutic molecules to cells is plasma membrane impermeability. We have recently developed an optical delivery method by facilitating membrane permeability and thus, allowing activation of delivered molecules. Moreover, the delivery of therapeutic genes and other molecules to specific cell types can be spatially controlled by this non-viral optical delivery system. The method utilizes Gold Nano Rods (GNRs) which are functionalized with specific antibody t*o* bind to targeted cell type. After intravitreal injection of functionalized GNRs along with the therapeutic gene, a low-power near-infrared (NIR) laser beam matched to the surface plasmon resonance (SPR) peak of the GNRs is applied. Fig. 1 depicts the components and various steps involved in the Nano-enhanced Optical delivery (NOD) of therapeutic genes to specific groups of cells. In this NOD approach, metallic (gold) nano-rods are functionalized with specific antibody via EDC chemistry to facilitate their binding to the membrane of the cells (Fig. 1A). SEM images of gold nanorods in solution and magnified image of a region are shown in Fig. 1B and Fig. 1C respectively. Due to the SPR absorption, the fGNRs attached to specific cell types create nano-hotspots making the cell membrane transiently permeable leading to transfection. Fig. 1D shows the schematics of targeted binding of antibody functionalized gold nanorods to specific retinal layers and expression of opsin (mCherry reporter) in bipolar cells upon light irradiation.

Kinetics of retinal layer-specific fGNR binding and clearance of fGNRs

In order evaluate the binding of antibody functionalized fGNRs to specific cell type, fluorescently tagged GNRs were functionalized with rod bipolar cell specific antibody (PKCα, Fig 2A). The PKCα antibody functionalized GNRs were intravitreally injected in wild type mice. After 1h, 1d and 1 week of injection, the mice were sacrificed and presence of fGNRs in different retinal layers was quantified by use of confocal fluorescence microscopy. The confocal imaging confirms the presence of fGNRs (Alexa Fluor 488 tagged) in the inner nuclear layer (INL) as reveled by the bright green fluorescence (middle panel of Fig. 1B). Minimal autofluorescence was observed in non-targeted retina layers (Top: ganglion cell layer, GCL and Bottom: outer nuclear layer, ONL). In the targeted INL layer, the peak binding and presence of the fGNRs were observed between 1d-1week of injection (Fig. 1B), which declined thereafter. It may be noted that the fGNRs (measured by fluorescence assay), which do not carry the therapeutic load (genes), are used to enhance the light intensity to deliver the therapeutic genes that are not attached to the fGNRs. The presence of fGNRs is not required once the light-based delivery is accomplished.

Quantitative analysis of fluorescence intensity (label for fGNRs) for different retinal layers at various time points show layer-specific binding. In Fig. 1C, we show kinetics of inner nuclear layer (INL) specific fluorescence. The increase in nanorod binding is observed to peak at 1 day after intravitreal injection and still lasts at 1 week (though at half of the peak value). Fig. 1D shows binding (assayed by fluorescence label intensity) of fGNRs in different layers after 1d of injection. The significantly higher specific binding in INL (i.e. Bipolar cells) is evident. Quantitative change in fGNR-label fluorescence for three different layers is shown in Fig. 1E. Longitudinal monitoring of fluorescence in different retinal layers shows that the presence of functionalized GNRs in the non-specific Ganglion cell and Outer Nuclear layers decreases rapidly within 1 day of injection.

Targeting multiple cell types by tuning of delivery laser wavelength

By use of aspect ratio of long to short axis of the functionalized field-enhancing gold nanorod (Suppl. Fig. 1), wavelength-selective narrow band optical enhancement could be achieved near cells. Thus, tuning the NIR laser wavelength allowed cell-selective delivery. For conducting NOD, 1 hour after injection of 1 μl of functionalized GNRs (inside eye concentration: 30 ng/μl), 1 μl of MCO-II-mCherry plasmid solution was injected intravitreally into *wild type* mice eye to result in final concentration of 50 ng/μl plasmids inside the vitreous cavity. To allow CW NOD laser beam irradiation of retina, the mouse eye was dilated with Tropicamide.

For RGC-specific delivery, intravitreal injection of Thy1-GNRs was carried out leading to effective binding to proximal RGC layer . MCO-II delivery to RGCs was achieved by 800 nm CW laser beam (30 mW, 60 s). One week after intravitreal injection and NOD, the mice were sacrificed, and retinal cup extracted and imaged using confocal fluorescence microscopy. Efficient transduction of MCO-II can be visualized by reporter-mCherry antibody staining (Green, Fig. 3A). The RGC membrane-specific MCO-II-mCherry expression by NOD is evident in Fig. 3A. The binding of RGC specific Thy1 antibody

functionalized GNRs with SPR peak at 780 nm (labeled with Alexa 555-Red) can be seen even at 1 week (though at reduced level).

Bipolar cell specific expression of MCO-II-mCherry was achieved by use of PKCα functionalized GNR (SPR peak at 850 nm) and 850 nm CW laser beam (power: 30 mW) irradiating 1 mm^2 area for 60 s (total dose =1800 mJ/mm^2). The mCherry expression in bipolar cell layers was confirmed by visualizing the antibody staining (Red). The specific binding of PKCα-GNRs to the bipolar cells could be seen in the fluorescence image of the labeled fGNRs (Alexa 488) in Green (Fig. 3B). Thus, triple selective optical delivery was achieved via cell-specific functionalization of gold nanorods, followed by spatially localized laser irradiation, wherein the delivery laser wavelength was tuned to SPR of GNRs.

No adverse changes in measured ERG and IOP due to NOD of MCO-II

To evaluate any adverse effect on ocular function due to NOD (injection of MCO-II plasmids, fGNRs and subsequent laser irradiation), longitudinal ERG measurements were carried out before and after optical delivery of MCO-II using 800 nm laser (Dose: 1800 mJ/mm^2: 30 mW, 60 sec) in wild type mice. After overnight dark adaptation, scotopic ERG responses to single white flash stimuli of increasing intensities (from 0.01 to 10 $cd{\cdot}s{\cdot}m^{-2}$) were recorded. The representative ERG profiles generated at different stimulation intensities for baseline, 1 week and 2 weeks after NOD are shown in Fig. 4A–C respectively. The a and b-waves were averaged from 20 consecutive traces for each intensity. Quantitative comparison of a-wave and b-wave amplitude at 3.0 cd. s/m^2 for baseline and different timepoints after optical delivery is shown in Fig. 4D and Fig. 4E respectively. No statistically significant change in a- and b-wave amplitude of scotopic ERG recording was observed implying that the rod and cone photoreceptors in wild type mice were not damaged by the optical delivery.

In order to evaluate laser-induced ocular hypertension (if any) or change due to fGNRs injection, intra ocular pressure (IOP) was measured before (baseline) and after NOD (2 weeks and 3 weeks). The change in IOP over time for individual mouse are shown in Fig 4F. No significant change in IOP from baseline was observed across the mice group over the 3-week period after NOD.

No detectable structural damage due to nano-enhanced optical delivery

Optical sectioning/imaging using SD-OCT was carried out to monitor any changes in ocular structure due to intravitreal injection of fGNRs, and MCO-II plasmids in mice. During intravitreal injection of fGNRs and MCO-II plasmids, there might be an injection related retinal damage (such as retinal detachment). Therefore, we evaluated structural integrity of retinal tissue and other ocular elements (cornea, lens) after injection, before optical delivery (Fig. 5A). Possible ocular damage can result from laser induced damage to retina or other elements and post-delivery retinal cytotoxicity due to fGNRs or MCO-II expression. In order to characterize any damage due to laser beam irradiation, the cornea and retina were imaged (Fig. 5B) 7d after 800 nm laser based optical delivery using dose (1800 mJ/mm^2: 30 mW, 60 sec). Comparison of average (over 20 measurements/eye) retinal thickness between baseline

and post-delivery shows that integrity of the retina was intact after MCO-II delivery (Fig. 5C).

Monitoring Gold nanorod binding and clearance from retina using SDOCT

The presence of the GNR was evident in OCT B-scan as shown in Fig. 5B and Suppl. Fig. 2. The optical thickness (refractive index * physical thickness) of retina was found to increase on Day 1 of injection, which leveled off to the baseline value after 7 days. The transient increase in optical thickness of retina is attributed to the increase in number of GNRs in vicinity of the retinal cells, owing to high effective refractive index of gold nanoparticle embedded retina (as compared to retina before GNR injection). Fig. 5D shows increase in contrast between targeted Ganglion Cell Layer (GCL) and Retina Pigment Epithelium (RPE) over time with peak at 7d. This implies increased binding of fGNRs to RGCs, which falls off at 2 weeks.

Biodistribution of intravitreally injected MCO-II plasmids subsequent to optical delivery

Following intravitreal injection of MCO-II plasmids, fGNRs and optical delivery, mice were sacrificed at 2 weeks after dosing for collection of tissue samples. Total DNA was extracted and biodistribution analysis of intravitreally injected MCO-II plasmids after optical delivery to retina was carried out using qPCR in non-targeted tissues (lung, liver, kidney, spleen, testis, Mandibular/Mesenteric Lymph nodes, heart and brain). Supplementary Fig. 3 shows the measured vector copy number (per ng of DNA). qPCR detection of sequences 2 weeks post-injection and optical delivery shows very small or non-detectable quantities of MCO-II DNA in non-targeted tissues.

Identification and distribution of fGNRs in-vivo visualized by SEM

Though gold nanoparticles are known to induce no retinal toxicity[44], and gold nanorods have very low cytotoxicity allowing their use in clinical trials[45,46,47]. Further, identification and distribution of fGNRs in retina were visualized by scanning electron microscopy (SEM) imaging. Fig. 6A shows the schematics illustration of the steps involved for preparing the retina sample for SEM imaging. SEM image of retina (Fig. 6B) shows the surface morphology of retina and presence of fGNRs on the retina surface. The back-scattered electron (BSE) image of fGNR-injected mouse eye showed distribution of fGNRs in patches of retina. Most of the nanorods (fGNRs) were found to be washed away during sample preparation for SEM imaging (Fig. 6C). By use of Energy Dispersive X-ray analysis, compositional information of one of the attached gold nanorod (marked by red arrow) was obtained (Fig. 6D). The characteristic elemental (gold) peak (Au Mα1) is visible in the EDX spectrum (Fig. 6D). The retinal areas without gold nanorods showed absence of the Au (gold) peak (Suppl. Fig. 4A), while the gold nanorod clusters attached to retina produced significantly higher Au Mα1 peak (Suppl. Fig. 4B). SEM imaging showed that GNRs were cleared from the retina 1 week after intravitreal injection (Suppl. Fig. 5).

Evaluation of apoptosis of retinal cells after in-vivo optical delivery of MCO-II evaluated by TUNEL assay

Though in the optical delivery experiment, low power infrared laser irradiation is used, the possibility of apoptotic cell death and DNA damage by laser micro-irradiation cannot be ruled out. The NIR laser beam wavelengths (800, 850 nm) used for optical delivery of MCO-II has negligible absorption coefficient in transparent ocular layers such as the cornea, lens, and neural retina. Further, absorption of vitreous humor at these laser wavelengths are minimal. In order to evaluate apoptotic cell death, TUNEL assay was performed on the NOD delivered mice retina. Confocal fluorescence image of TUNEL positive cells (in green channel), and TUNEL-negative control cells are shown in Fig. 7A and 7B respectively as reference. Propidium Iodide staining for cell nuclei are shown in red channel. To evaluate safety of *in-vivo* NOD based MCO-II delivery, we used laser dose of at 1800 mJ/mm^2 (30 mW, 60 sec). Representative fluorescence images of mouse retina after 1 wk of intravitreal injection of fGNRs and MCO-II plasmids with laser delivery in OD eye are shown in Fig. 7C. Fig. 7D shows TUNEL staining of OS eye (injected with fGNRs and MCO-II plasmids) which did not receive laser irradiation. Quantification of TUNEL +ve cells for different experimental condition (OD: +Laser, OS: −Laser) shows no significant TUNEL positive cells in optically delivered (OD) eyes or contralateral eye. Further, there was no significant differences in apoptotic cell count between OD or OS retinas.

Discussion

Viral vectors for gene delivery are known to spread beyond targeted organ (for example to eye contralateral to injected eye) and gene transduction in target layer is known to be not localized. Here we demonstrated that field enhancement by gold nanorods for transiently perforating cell membrane to allow gene (MCO-II) delivery is minimally invasive and does not lead to apoptotic cell death in retina. We achieved targeted high throughput delivery of MCO-II plasmids in retina in-vivo. Non-viral optical delivery will allow multiple dosing without immunotoxicity and immune rejection (as encountered in viral delivery) with controlled expression. The key advantage of this nano-enhanced optical delivery includes increased sensitivity of targeted cells only (less collateral damage) to irradiation light. In addition, SPR of fGNRs in the NIR spectrum allows use of low optical power outside the visible spectrum, thus minimizing tissue damage due to ambient visible light exposure. Thus, compact, easy-to-use and safe low power lasers can be used to achieve targeted optical delivery. The safety and efficacy of the optical delivery method was demonstrated via electrophysiology (ERG), structural (OCT) imaging, TUNEL assay, immunostaining and confocal microscopy. The spatially targeted efficient non-delivery of MCO-II genes to geographic atrophic areas of dry-AMD [48–50] will allow re-photosensitization of the degenerated retina.

This method can achieve ubiquitous or have tropism for cell-specific delivery by use of functionalized gold nanorods as demonstrated here for bipolar and retinal ganglion cells in retina. Wavelength-selective enhancement near cells and multiplexing is achieved by tuning the NIR laser wavelength to shape (and surface plasmon resonance) of the functionalized gold nanorods. The aspect ratio (ratio of size of short axis to long axis) of gold nanorods

(GNRs) can vary from 1:1 to 1:5 to result in Surface plasmon resonance (SPR) peak varying from visible (~530 nm) to NIR (~1100 nm). Our earlier studies using this spatially-targeted method[42] demonstrated non-specific gene delivery limited to only RGC layer which is proximal to the intravitreal injection site. Functionalization of GNRs with different cell-specific antibodies allowed us to achieve gene transfer into deeper targeted-layer (inner nuclear layer). The cell selective optical delivery can be further increased by use of cell-specific promoter in the plasmid construct in addition to cell-specific functionalization of gold nanorods. While two different (Thy1 and PKCα) antibodies were used to target RGCs and bipolar cells, the targeting agents can be ligands, antibody fragments, nucleic acids, aptamers, small molecules, which is able to bind specifically to one cell type. Further, by careful choice of route of administration of GNRs enhances the cell-specific binding probability. In case of ocular delivery, while intravitreal injection is shown here to be effective for RGC and bipolar cell transduction, use of sub-retinal injection may be required for delivery to outer nuclear layer and retinal pigment epithelial cells.

Conclusions

Triple selective optical delivery of MCO-II plasmids was achieved via (i) cell-specific functionalization of gold nanorods, (ii) Spatially localized laser irradiation, and (iii) delivery laser wavelength tuned to SPR of GNRs. Kinetics of retinal layer-specific functionalized gold nanorods binding shows decline after one week and expected to clear through the excretory system. Longitudinal OCT measurement shows fGNR binding to targeted retinal layer and no detectable ocular damage after optical delivery. Quantification of MCO-II sequences two weeks after optical delivery showed very small or non-detectable quantities of MCO-II plasmids in tissues outside of the treated eyes. No adverse effect due to optical delivery was observed in longitudinal ERG and IOP measurements. Further, TUNEL assay-based evaluation showed that the retinal cells do not undergo apoptotic death after in-vivo optical delivery of MCO-II plasmids. Our results clearly demonstrate gene delivery and functional cellular expression in targeted regions of retina using CW NIR laser beam without apoptosis. Safe NOD-mediated molecular-delivery has potential for effective gene therapy of diverse retinal degenerations in patients.

Materials and Methods

Ethics statement

All experimental procedures were conducted according to the Nanoscope Technologies-Institutional Animal Care and Use Committee approved protocol.

Preparation of MCO-II Plasmids

High throughout DNA synthesizer were used to synthesize the parent DNA fragment coding for multi characteristic opsin-II (MCO-II)[42] with the restriction enzymes BamH1 and Sal1. The gene was built using a pAAV vector with CAG promotor, trafficking signal sequence and fluorescent reporter protein (mCherry). Amplification and purification of plasmid DNA of MCO-II-mCherry was carried out for optical delivery. The vector DNA construct was confirmed with restriction digestion and DNA gel electrophoresis.

Functionalization of Gold Nanorods

In order to evaluate layer specific delivery into ganglion cells, the GNRs with SPR peak of 780 nm were functionalized with Thy1 antibody. Thy-1-Carboxyl-GNR solution was prepared by first mixing 1ml of MES (25 mM), Carboxyl-GNR (50 μl), Thy-1 antibody solution (50 μl), and EDC (3.8 mg). The mixture was incubated for 90 min at room temperature and centrifuged for 7 min at 9,000 rpm. The supernatant was discarded, resuspended with 2% PEG solution in 1xPBS (100ul) and stored at 4oC until use. For Bipolar cell specific optical delivery, GNRs with SPR peak of 850 nm were functionalized with PKCα antibody following the method described above for Thy-1-Carboxyl-GNRs.To minimize non-specific binding, the GNRs are PEGylated. PEGylation also prevents the aggregation of the GNRs.

Mice model with Retina degeneration

Retinal degenerated mice (B6.CXB1-*Pde6b*^{rd10}/J) and wild type (C57BL/6J) were obtained from Jackson laboratory and bred in the animal facilities of the Nanoscope Technologies. Retinal degenerated (*rd10*) mice (B6.CXB1-Pde6brd10/J) have a spontaneous missense point mutation in Pde6b (cGMP phosphodiesterase 6B, rod receptor, beta polypeptide) which leads to later onset and slower retinal degeneration similar to human disease. The mice were maintained on a 12:12 light cycle. All aspects of experimental procedures on the animals were in strict accordance with guidelines of the Nanoscope Technologies Institutional Animal Care and Use Committee (IACUC). Mice were maintained on a 12:12 light cycle.

Randomization and Masking

Randomized block experimental design was implemented in order to ensure that different treatments are assigned to each experimental group with a known, equal probability of receiving a given treatment. Mice were selected randomly, and group number/cage number/mice number were assigned prior to injection based on restricted randomization. The cages were housed in a random order on the shelves and the injections were done in random order.

To avoid bias, the imaging experiments and analysis were performed by individuals masked with respect to the treatments. After the randomized allocation of animals to the treatments, animals, samples, and treatments were coded until the data were analyzed.

Intravitreal injection of fGNRs and MCO-II plasmids

Aseptic technique was used for all surgical procedures and surgical tools were sterilized with autoclave. The mouse was anesthetized and local anesthesia (proparacaine) was instilled into the eye of the animal. The fGNRs (SPR at 780 or 850 nm) or MCO-II plasmid solution (1 μl) was injected by a sterilized 32-gauge needle of a Hamilton micro-syringe inserted through the sclera into the vitreous cavity (intravitreal injection) under a dissection microscope. The cornea was kept moist with a balanced salt solution during the surgical procedure. Ciprofloxacin 0.3% eye drops were applied to the ocular surface following the intravitreal injection.

Laser irradiation for optical delivery of MCO-II-mCherry plasmids

Prior to the optical delivery of MCO-II plasmids, the mice were anesthetized using the mixture of 90 mg/kg ketamine, 10 mg/kg xylazine and 0.5 mg/kg acepromazine. Tropicamide (1%) was used to dilate the pupils of the mice. Sterile Proparacaine hydrochloride ophthalmic solution of 0.5% eyedrops were administered to provide topical anesthesia. The mouse was placed under a dissection microscope and the eye was imaged via the eyepiece camera. After intravitreal injection of MCO-II plasmids, the targeted retinal area was irradiated by a near-infrared (800 or 850 nm) laser beam coupled through one of the eyepieces of the dissection microscope. The power and exposure time of the laser beam was controlled. The cornea was kept moist with a balanced salt solution during the optical delivery procedure. Reversal of anesthetic was achieved by intraperitoneal injection of normal sterile 0.9% saline solution (400 μl).

Immunostaining of retina

The NOD treated and non-treated samples (mice retinas) were fixed in 4% PFA in 1xPBS for15 min at room temperature and washed with 1x PBS and 0.5% triton x-100 (washing solution) three times. The nonspecific binding of antibodies was blocked by 4% serum for 60 min and washed with washing solution three times. The samples were incubated with primary antibodies (1: 500 dilution), e.g., anti-mCherry. After washing samples with 0.5% TritonX-100 solution in 1xPBS three times, secondary antibody (Goat anti rabbit Alexa 488 nm or Goat anti mouse Alexa 594 nm), diluted 1:250 in washing solution, was loaded for one hour at room temperature. The samples were then stained with DAPI (1: 200 dilution).

TUNEL (Transferase dUTP Nick End Labeling) Assay

The TUNEL assay is widely used for the detection of apoptosis. TUNEL assay was carried out using APO-BRDU (TUNEL) Apoptosis Kit (Novus Biological). Addition of Br-dUTP catalyzed by TdT to the 3’-OH sites of DNA strand breaks in the genome allows detection of apoptotic cells. The experiment on retina was performed following manufacturer’s instructions.

Confocal Fluorescence imaging

Confocal microscopic imaging was carried out for: (i) monitoring fluorescently labeled functionalized gold nanorods, (ii) MCO-II-mCherry expression after optical delivery, and (iii) TUNEL assay. The explanted retinal tissues were immuno-stained to identify and quantify mCherry (reporter) expression. Prior to imaging, the samples were washed with 1xPBS. Images were taken by confocal microscope (Olympus Fluoview FV1000) using the laser with excitation lines at 405 nm (DAPI), 488 nm (Alexa 488) and 543 nm (Alexa 594). Image processing was performed using ImageJ software.

DNA extraction and qPCR Analysis

Genomic DNA was extracted from tissue samples using GeneJET Genomic DNA Purification Kit (ThermoFisher) according to the manufacturer’s protocol and diluted to a concentration of 10 ng/μL. Melting curve analysis was performed to ensure single-product amplification for the primer pair. qPCR was performed using Takara AAVproTM Titration

kit standard (cat# 6233) and Fisher Scientific Company's Master Mix, qPCR (Applied Biosystems) and Power Up SYBR Green Master Mix (cat# A25776). 50X Primer Mix was prepared as follows: AAV Forward ITR Primer 5µl, AAV Reverse ITR primer 5 µl, water 15 µl. The qPCR reaction mix consisted of: SYBR green Premix 12.5 µl, 50X Primer Mix 0.5 µl, water 7 µl, template DNA (~10 ng) 5µl. Primers for the ITR (part of MCO gene) was used. Real time PCR was performed on the Applied Biosystems QuantStudio 3 real time PCR System (Applied Biosystems) using assays specific for ITR. Samples were analyzed in duplicate for vector copy number/ng DNA by the Absolute Quantification method using standard curves. Preparation of the standard curve was performed following the manufacturer's reference guide.

Optical Coherence Tomographic (OCT) imaging

The mice were anesthetized with a mixture of ketamine (65 mg/kg), xylazine (7.5 mg/kg), and acepromazine (0.5 mg/kg) and mounted on a maneuverable imaging platform. 1~2 drops of 1% tropicamide was topically applied to eyes for pupil dilation. The cornea was kept moist with a balanced salt solution during the measurement period. Spectral Domain-OCT (SD-OCT) imaging[51–53] (NS-Ray; Nanoscope Instruments) was performed before and after 1,2 weeks of intravitreal injection and optical delivery. Retinal thickness and contrast measurements were made at different locations of the retina before and after optical delivery.

Intra Ocular Pressure (IOP) measurement

For IOP measurement, the mouse was placed on a wire cage and allowed ~1 min of resting time. The tonometer (Tonovet Plus, iCARE) was loaded with a new probe allowing it for self-calibration. The Tonovet was positioned parallel to the eye with a distance of about half an inch and aimed to the center of the cornea. Three trials of IOP measurement were carried out, each trial consisting of 6 readings.

ERG measurement

For scotopic ERG measurement, mice were dark-adapted overnight. Mice were anesthetized as described previously by use the mixture of 90 mg/kg ketamine, 10 mg/kg xylazine and 0.5 mg/kg acepromazine. Prior to electrical recording, 1% Tropicamide was topically applied to the mouse eye for pupil dilation. The mouse was placed on a heating pad set to ~35°C. The ground needle electrode was placed into the tail and a reference needle electrode was placed sub-dermally between the eyes. The silver wire contact lens electrode was used as a recording electrode. The light stimulation intensity was varied from 0.01 to 10 cd-s/m^2. For each stimulation intensity, 20 light-evoked electrical responses were recorded by Espion E3 (Diagnosys LLC) and averaged.

Statistics

GraphPad Prism was used to analyze data. The data were plotted as mean ± S. D or Mean± SEM. Statistically significant difference analyses were carried out by t-test. $P < 0.05$ was considered statistically significant.

Supplementary Material

Refer to Web version on PubMed Central for supplementary material.

Acknowledgements

The authors would like to acknowledge supports from the National Institute of Health (1R43EY026483-01, 1R43EY025905-01, 1R01EY025717-01A1, 1R01EY028216-01A1, 2R44EY025905-02A1). The authors would also like to thank Rod Baird and Takeshi Sunaoshi (Hitachi) for SEM imaging and EDX analysis and Ms. Laura Marquez (Nanoscope) for animal care.

References

1. Luo D & Saltzman WM Synthetic DNA delivery systems. Nat Biotech 18, 33–37 (2000).
2. Yu J-Y, DeRuiter SL & Turner DL RNA interference by expression of short-interfering RNAs and hairpin RNAs in mammalian cells. Proc. Nat. Acad. Sci 99, 6047–6052 (2002). [PubMed: 11972060]
3. Burridge K & Feramisco JR Microinjection and localization of a 130K protein in living fibroblasts: a relationship to actin and fibronectin. Cell 19, 587–595 (1980). [PubMed: 6988083]
4. Akilov OE, et al. Vaccination with photodynamic therapy-treated macrophages induces highly suppressive T-regulatory cells. Photodermatol., Photoimmunol. Photomed 27, 97–107 (2011). [PubMed: 21392113]
5. Somia N & Verma IM Gene therapy: trials and tribulations. Nat Rev Genet 1, 91–99 (2000). [PubMed: 11253666]
6. Verma IM & Somia N Gene therapy - promises, problems and prospects. Nature 389, 239–242 (1997). [PubMed: 9305836]
7. Wu Z, Yang H & Colosi P Effect of genome size on AAV vector packaging. Molecular Therapy 18, 80–86 (2010). [PubMed: 19904234]
8. Carter M & Shieh JC Guide to research techniques in neuroscience, (Academic Press, 2015).
9. Miller DG, Adam MA & Miller AD Gene transfer by retrovirus vectors occurs only in cells that are actively replicating at the time of infection. Mol.Cell Biol 10, 4239–4242 (1990). [PubMed: 2370865]
10. Ragot T, et al. Efficient adenovirus-mediated transfer of a human minidystrophin gene to skeletal muscle of mdx mice. Nature 361, 647–650 (1993). [PubMed: 8437625]
11. Alexander IE, Russell DW, Spence AM & Miller AD Effects of gamma irradiation on the transduction of dividing and nondividing cells in brain and muscle of rats by adeno-associated virus vectors. Hum. Gene Ther 7, 841–850 (1996). [PubMed: 8860836]
12. Paoletti E Applications of pox virus vectors to vaccination: an update. Proc.Natl.Acad.Sci U.S.A 93, 11349–11353 (1996). [PubMed: 8876138]
13. Herz J & Gerard RD Adenovirus-mediated transfer of low density lipoprotein receptor gene acutely accelerates cholesterol clearance in normal mice. Proc.Natl.Acad.Sci U.S.A 90, 2812–2816 (1993). [PubMed: 8464893]
14. Simon RH, et al. Adenovirus-mediated transfer of the CFTR gene to lung of nonhuman primates: toxicity study. Hum.Gene Ther 4, 771–780 (1993). [PubMed: 7514446]
15. Ali M, Lemoine NR & Ring CJ The use of DNA viruses as vectors for gene therapy. Gene Ther. 1, 367–384 (1994). [PubMed: 7584103]
16. Wu Z, Yang H & Colosi P Effect of genome size on AAV vector packaging. Mol.Ther 18, 80–86 (2010). [PubMed: 19904234]
17. Newman CM, Lawrie A, Brisken AF & Cumberland DC Ultrasound Gene Therapy: On the Road from Concept to Reality. Echocardiography 18, 339–347 (2001). [PubMed: 11415507]
18. Li S & Huang L Nonviral gene therapy: promises and challenges. Gene Ther 7, 31–34 (2000). [PubMed: 10680013]

19. Templeton NS, et al. Improved DNA: liposome complexes for increased systemic delivery and gene expression. Nat Biotech 15, 647–652 (1997).
20. King R Gene Delivery to Mammalian Cells by Microinjection. Methods in Molecular Biology 245, 167–173 (2004). [PubMed: 14707377]
21. Ferber D Safer and Virus-Free? Science 294, 1638–1642 (2001). [PubMed: 11721029]
22. Panyam J & Labhasetwar V Biodegradable nanoparticles for drug and gene delivery to cells and tissue. Adv. Drug Deliv. Rev 55, 329–347 (2003). [PubMed: 12628320]
23. Bordet T & Behar-Cohen F Ocular gene therapies in clinical practice: viral vectors and nonviral alternatives. Drug discovery today 24, 1685–1693 (2019). [PubMed: 31173914]
24. Mohan RR, Rodier JT & Sharma A Corneal gene therapy: basic science and translational perspective. The ocular surface 11, 150–164 (2013). [PubMed: 23838017]
25. Hauswirth WW & Beaufrere L Ocular gene therapy: quo vadis? Investigative ophthalmology & visual science 41, 2821–2826 (2000). [PubMed: 10967033]
26. Grunwald JE, et al. Growth of Geographic Atrophy in the Comparison of Age-related Macular Degeneration Treatments Trials. Ophthalmology (2014).
27. Nagel G, et al. Channelrhodopsin-2, a directly light-gated cation-selective membrane channel. Proc. Nat. Acad. Sci 100, 13940–13945 (2003). [PubMed: 14615590]
28. Boyden ES, Zhang F, Bamberg E, Nagel G & Deisseroth K Millisecond-timescale, genetically targeted optical control of neural activity. Nat Neurosci 8, 1263–1268 (2005). [PubMed: 16116447]
29. Aravanis AM, et al. An optical neural interface: in vivo control of rodent motor cortex with integrated fiberoptic and optogenetic technology. Journal of Neural Engineering 4, S143–156 (2007). [PubMed: 17873414]
30. Zhang F, Aravanis AM, Adamantidis A, de Lecea L & Deisseroth K Circuit-breakers: optical technologies for probing neural signals and systems. Nat Rev Neurosci 8, 577–581 (2007). [PubMed: 17643087]
31. Pastrana E Optogenetics: controlling cell function with light. Nat Meth 8, 24–25 (2011).
32. Johansen JP, et al. Optical activation of lateral amygdala pyramidal cells instructs associative fear learning. Proc. Nat. Acad. Sci 107, 12692–12697 (2010). [PubMed: 20615999]
33. Tønnesen J, et al. Functional Integration of Grafted Neural Stem Cell-Derived Dopaminergic Neurons Monitored by Optogenetics in an In Vitro Parkinson Model. PLoS ONE 6, e17560 (2011). [PubMed: 21394212]
34. Adamantidis AR, et al. Optogenetic interrogation of dopaminergic modulation of the multiple phases of reward-seeking behavior. J Neurosci 31, 10829–10835 (2011). [PubMed: 21795535]
35. Alilain WJ, et al. Light-Induced Rescue of Breathing after Spinal Cord Injury. J. Neurosci 28, 11862–11870 (2008). [PubMed: 19005051]
36. Ivanova E, Roberts R, Bissig D, Pan Z-H & Berkowitz BA Retinal channelrhodopsin-2-mediated activity in vivo evaluated with manganese-enhanced magnetic resonance imaging. J. Molecular. Vision 16, 1059–1067 (2010).
37. Lagali PS, et al. Light-activated channels targeted to ON bipolar cells restore visual function in retinal degeneration. Nat. Neurosci 11, 667–675 (2008). [PubMed: 18432197]
38. Shivalingaiah S, Gu L & Mohanty SK Correlation of spatial intensity distribution of light reaching the retina and restoration of vision by optogenetic stimulation. Proc. SPIE 7885, 78851Y (2011).
39. Busskamp V, Picaud S, Sahel J-A & Roska B Optogenetic therapy for retinitis pigmentosa. Gene therapy 19, 169–175 (2012). [PubMed: 21993174]
40. Gaub BM, et al. Optogenetic retinal gene therapy with the light gated GPCR vertebrate rhodopsin. in Retinal Gene Therapy 177–189 (Springer, 2018).
41. Henriksen BS, Marc RE & Bernstein PS Optogenetics for retinal disorders. Journal of ophthalmic & vision research 9, 374 (2014). [PubMed: 25667740]
42. Batabyal S, et al. Near-infrared laser based spatially targeted nano-enhanced optical delivery of therapeutic genes to degenerated retina. Molecular Therapy-Methods & Clinical Development (2020).

43. Batabyal S, Gajjeraman S, Bhattacharya S, Wright W & Mohanty S Nano-enhanced optical gene delivery to retinal degenerated mice. Current Gene Therapy 19, 318–329 (2019). [PubMed: 31625475]
44. Kim JH, Kim JH, Kim K-W, Kim MH & Yu YS Intravenously administered gold nanoparticles pass through the blood–retinal barrier depending on the particle size, and induce no retinal toxicity. Nanotechnology 20, 505101 (2009). [PubMed: 19923650]
45. Kumthekar P NU-0129 in Treating Patients With Recurrent Glioblastoma or Gliosarcoma Undergoing Surgery. (2017).
46. Dayan CM Enhanced Epidermal Antigen Specific Immunotherapy Trial -1 (EE-ASI-1). (2016).
47. Gabinsky J Plasmonic Nanophotothermal Therapy of Atherosclerosis (NANOM-FIM). (2011).
48. Klein ML, et al. Progression of geographic atrophy and genotype in age-related macular degeneration. Ophthalmology 117, 1554–1559, 1559 e1551 (2010). [PubMed: 20381870]
49. Fleckenstein M, et al. Tracking progression with spectral-domain optical coherence tomography in geographic atrophy caused by age-related macular degeneration. Invest Ophthalmol Vis Sci 51, 3846–3852 (2010). [PubMed: 20357194]
50. Sunness JS, Applegate CA, Bressler NM & Hawkins BS Designing clinical trials for age-related geographic atrophy of the macula: enrollment data from the geographic atrophy natural history study. Retina 27, 204–210 (2007). [PubMed: 17290203]
51. Liu Y, et al. Monitoring retinal morphologic and functional changes in mice following optic nerve crush. Invest Ophthalmol Vis Sci 55, 3766–3774 (2014). [PubMed: 24854856]
52. Kim BJ, et al. In vitro and in vivo neuroprotective effects of cJun N-terminal kinase inhibitors on retinal ganglion cells. Mol Neurodegener 11, 30 (2016). [PubMed: 27098079]
53. Kim BJ, Sprehe N, Morganti A, Wordinger RJ & Clark AF The effect of postmortem time on the RNA quality of human ocular tissues. Mol Vis 19, 1290–1295 (2013). [PubMed: 23805035]

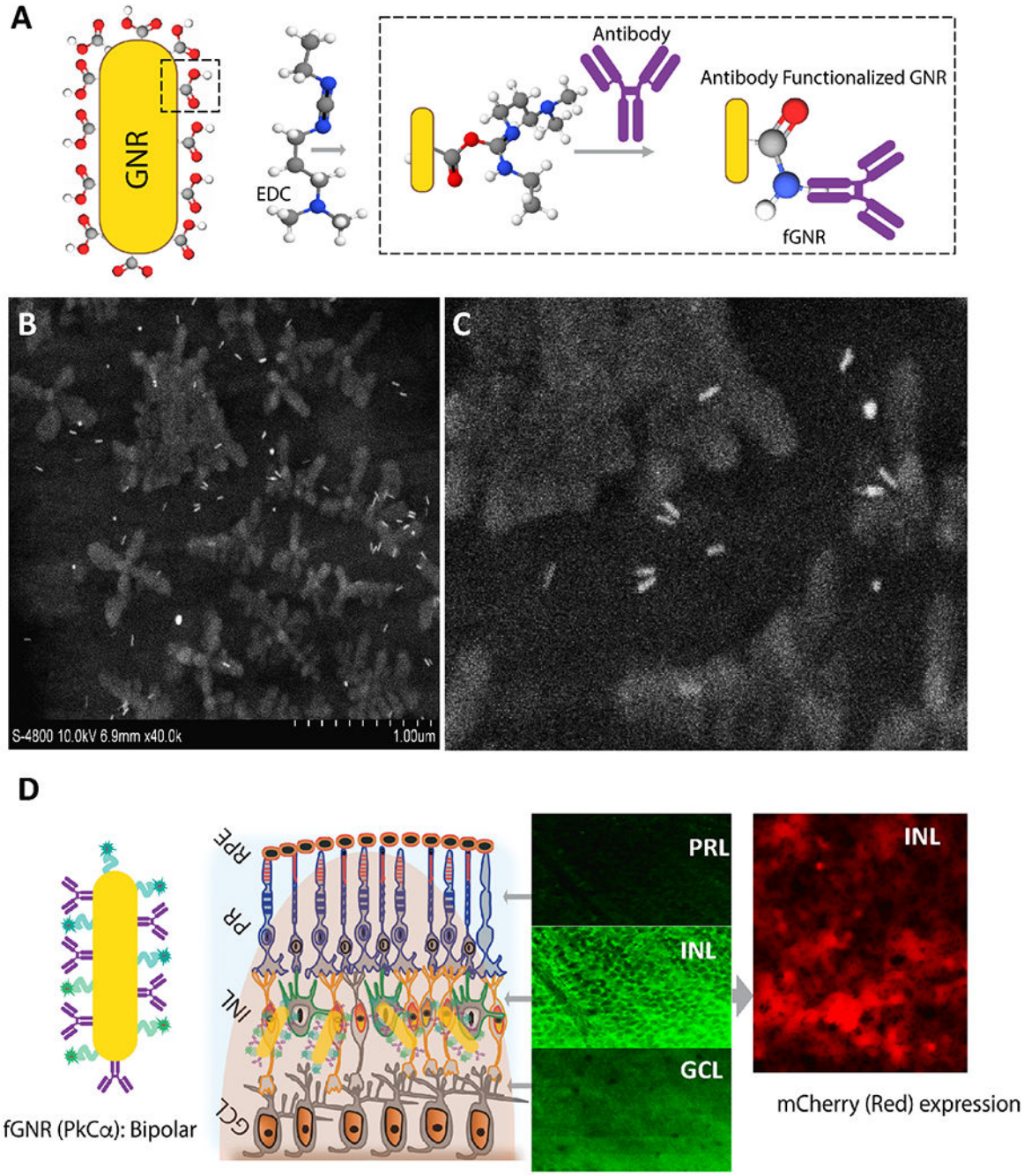

Fig. 1. Graphical illustration of nano-enhanced optical delivery.

(A) Two-step surface functionalization of GNR using specific antibody to targeted retina binding. (B) Scanning electron microscope image of functionalized gold nanorods, (C) zoomed picture showing individual nanorods. (D) Schematics of targeted binding of antibody functionalized gold nanorods to specific retinal layers and expression of opsin (and mCherry reporter) upon light irradiation due to fGNR-based enhancement of light intensity in the vicinity of targeted cells. ONL: Outer Nuclear Layer; INL: Inner Nuclear layer; and GCL: Ganglion Cell Layer.

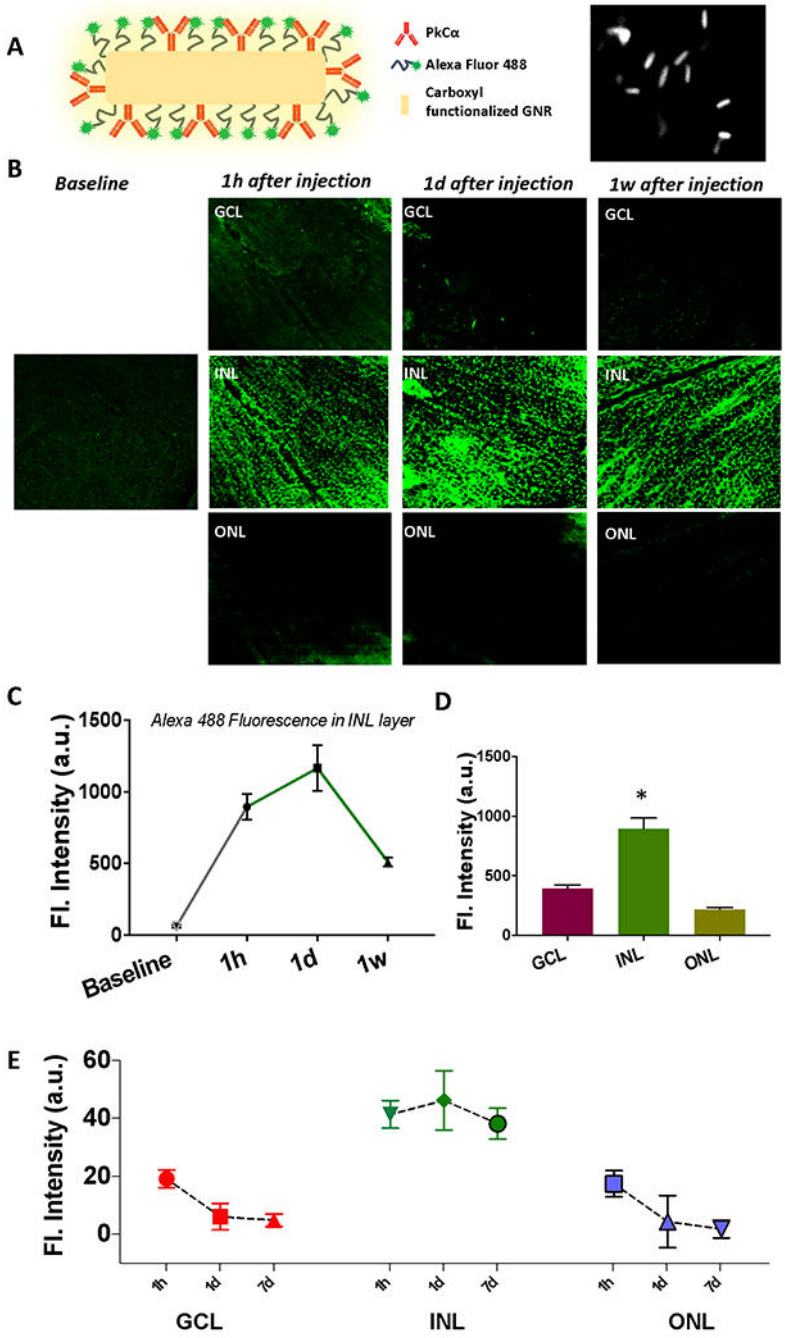

Fig. 2. Kinetics of retinal layer-specific fGNR binding shows peak after 1d of injection, which declines after 1 wk.

(A) Schematic of fGNR functionalized with PKCα antibody for bipolar cell specific binding along with SEM image of fGNRs. (B) Layer-specific binding of fGNRs after 1 hour, 1 day and 1 week of intravitreal injection in mice. Z-section of confocal microscopy imaging reveals the highest presence of GNR in the inner nuclear layer (except in baseline) compared to other retinal layers (such as ganglion cell layer and photoreceptor layer). (C) Change in layer-specific fluorescence (fluorescent tagged fGNRs) over time in INL layer (baseline fluorescence of the INL layer is before injection of GNRs). (D) Layer-specific binding

of fGNRs after 1d of injection. (E) Longitudinal monitoring of functionalized GNRs in different retinal layer. N=3 animals. *p<0.05.

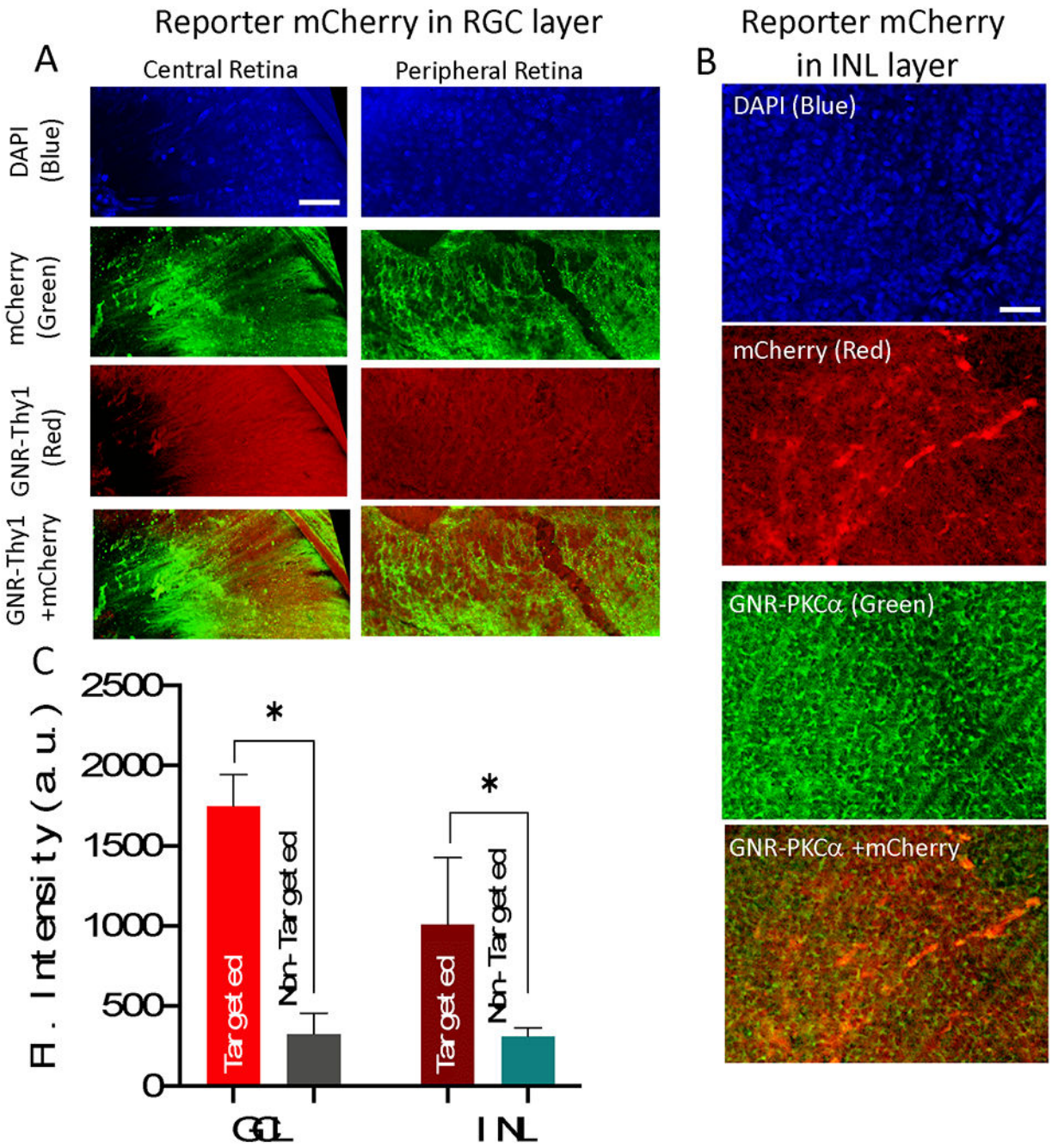

Fig. 3. Triple selective optical delivery via (i) cell-specific functionalization of gold nanorods, (ii) Spatially localized laser irradiation, and (iii) delivery laser wavelength tuned to SPR of GNRs.

(A) RGC specific Thy1 antibody functionalized GNRs (labeled with Alexa 555-Red), MCO expression achieved by 800 nm CW laser (30 mW, 60 s) visualized by mCherry antibody staining (Green), 1 week after gene delivery. (B) Bipolar cell specific PKCα antibody functionalized GNRs (labeled with Alexa 488-Green), ON-bipolar cell specific MCO expression achieved by 850 nm CW laser (total dose =1800 mJ/mm^2: 30 mW for 60 sec, 1 mm^2 area) visualized by antibody staining (Red), 1 week after gene delivery. Scale

bar: 50 μm. (C) The quantitative comparison of MCO (mCherry reporter) expression in RGC layer and INL versus non-targeted area. N=3 animals. *p<0.05

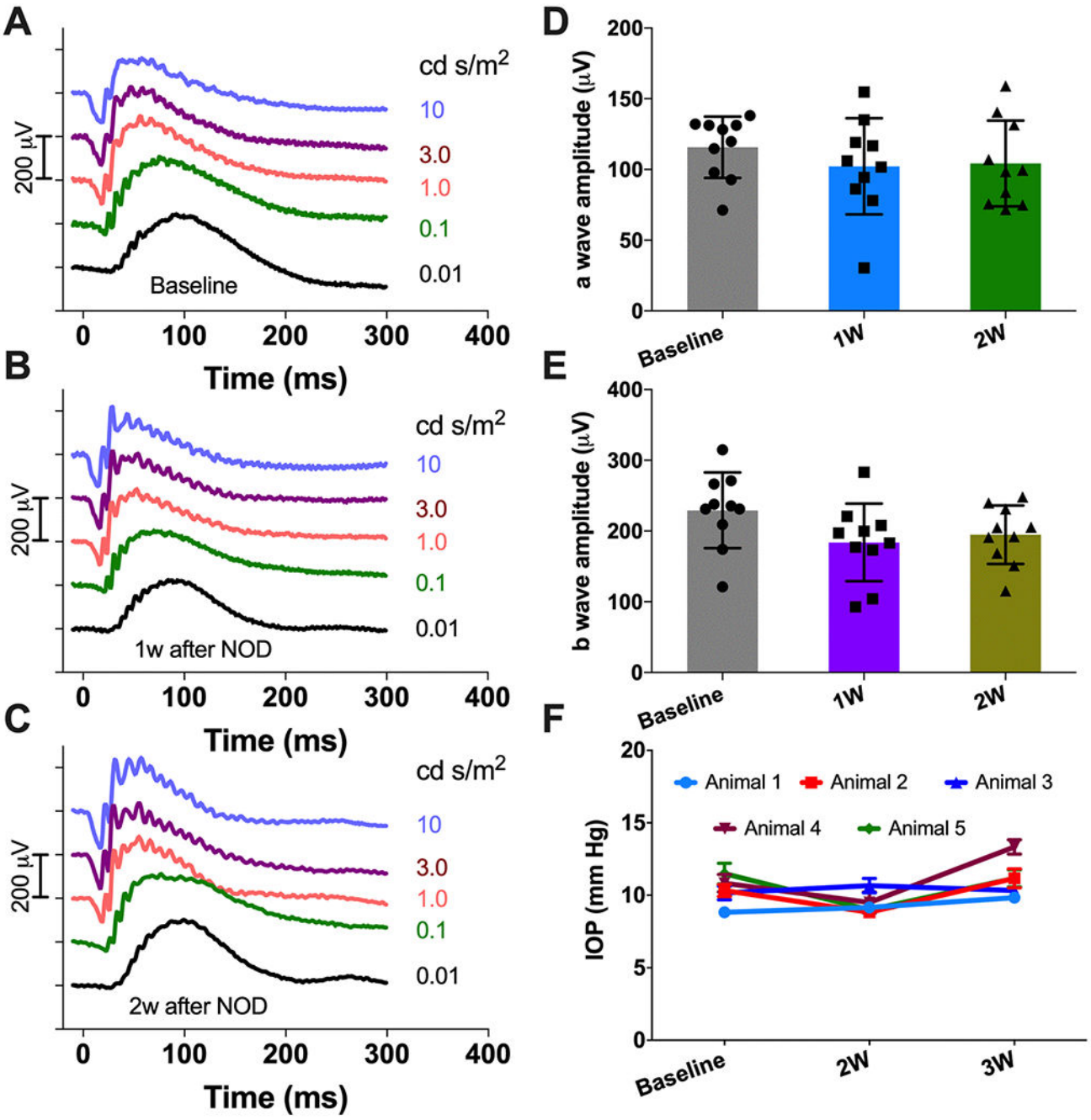

Fig. 4. No adverse effect due to NOD observed in longitudinal ERG and IOP measurements in wild type mice.

Representative visual stimulation evoked ERG profile of wild type mice: (A) Baseline; (B) 1 wk and (C) 2 wk after NOD. Flash intensities are indicated in cd.s/m^2. Quantitative comparison of (D) a-wave and (E) b-wave amplitude at 3.0 cd.s/m^2. Av. ± S.D. The a and b-waves were averaged from 20 consecutive trace for each intensity. (F) Longitudinal IOP measurements showing no significant change in IOP value for the individual animals before and after NOD (N=5 animals). Av. ± S.E.M.

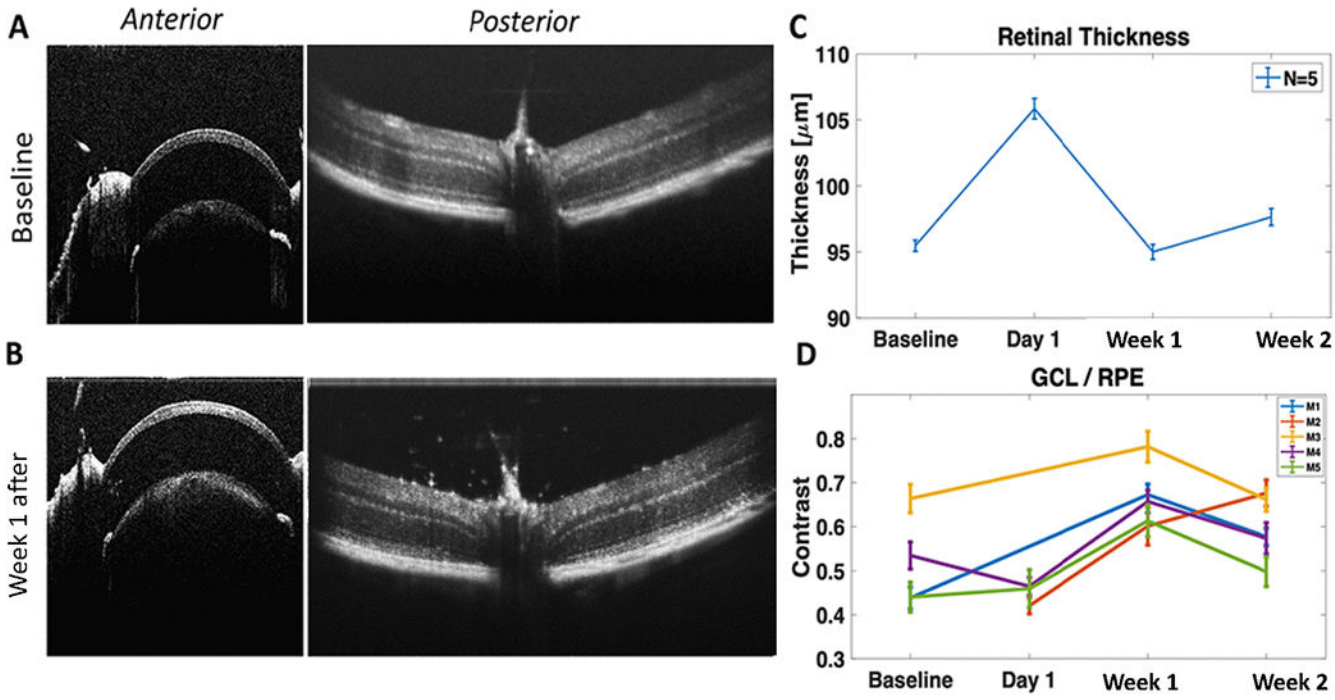

Fig. 5. Longitudinal OCT measurement shows no detectable ocular damage after optical delivery and fGNR binding/clearance to targeted retinal layer.

OCT images of cornea and lens (and iris) and retina (A) before, and (B) 1 week after optical delivery using dose (1800 mJ/mm^2: 30 mW, 60 sec, 1 mm^2 area). (C) Comparison of optical thickness of retina (Before injection vs. After intravitreal injection and optical delivery). (D) Change of contrast between Ganglion Cell Layer (GCL) and Retina Pigment Epithelium (RPE) over time. N=5 animals. Av ± SEM.

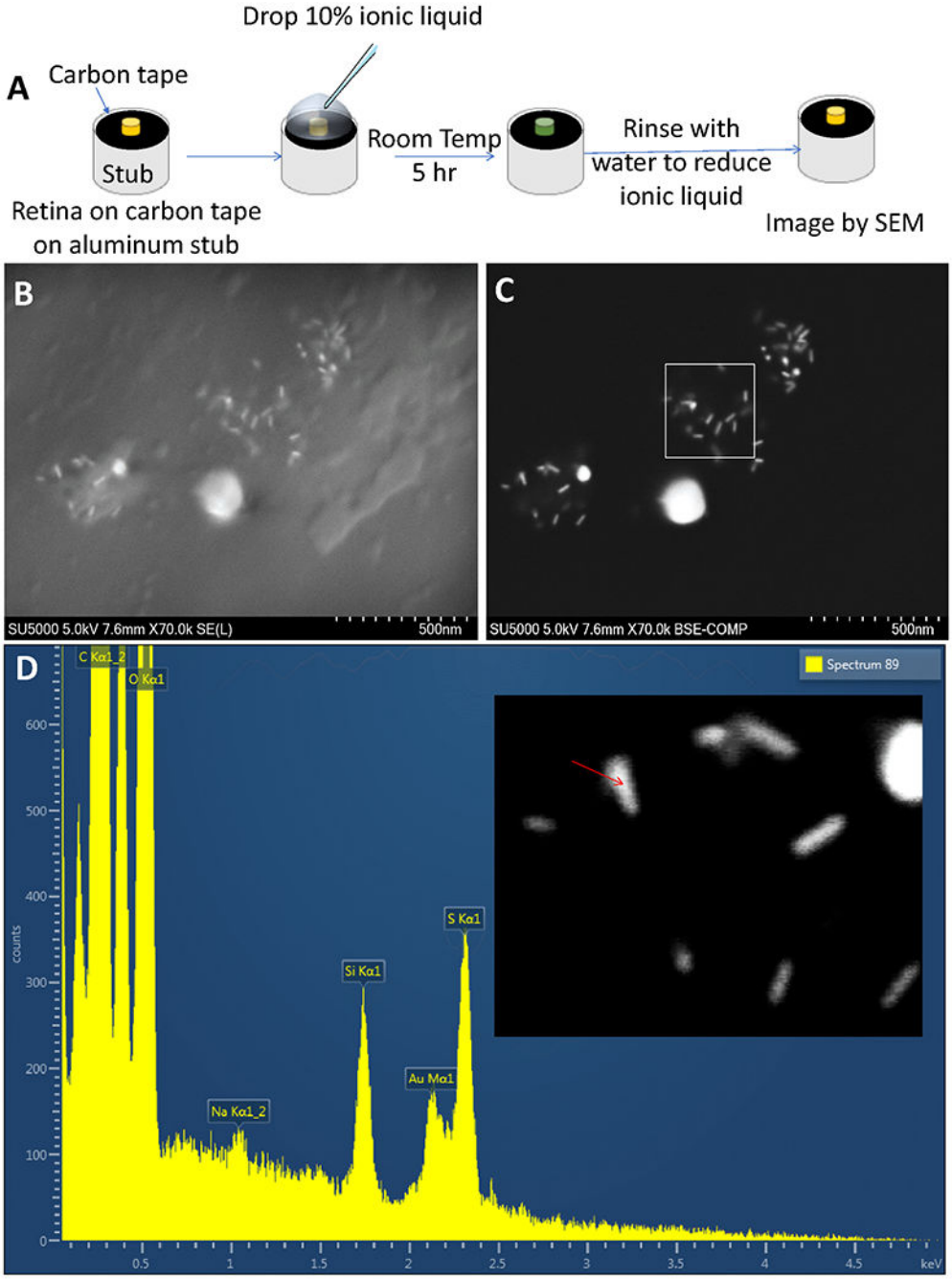

Fig. 6. Identification and distribution of fGNRs in-vivo visualized by scanning electron microscopy imaging.

(A) Schematics illustration of the steps involved for imaging the NOD eye cup. (B) Scanning electron microscope image revealing the surface morphology and presence of fGNRs on the retina surface. (C) Back-scattered electron (BSE) image of fGNR-injected mouse eye showing distribution of fGNRs. (D) Compositional information of an attached gold nanorod (marked by red arrow) obtained via Energy Dispersive X-ray analysis.

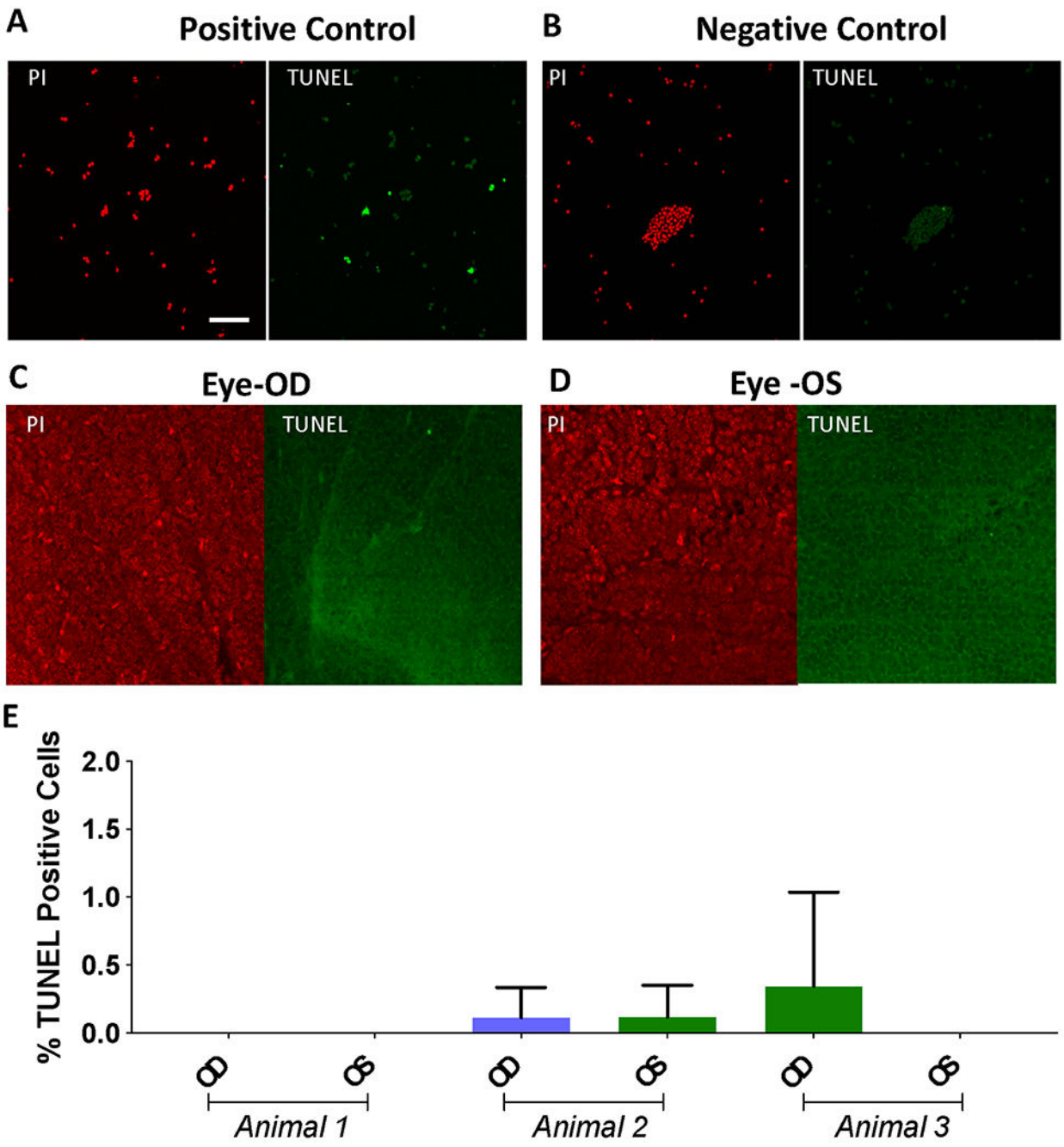

Fig. 7. TUNEL assay to evaluate apoptosis of retinal cells after in-vivo optical delivery of MCO-II.

Confocal fluorescence image of (A) TUNEL positive cells (in green channel, Propidium Iodide in red channel showing cell nuclei), and (B) TUNEL-Negative control cells. Representative fluorescence images of *rd10* mouse retina after 1 wk of intravitreal injection of fGNRs and MCO-II plasmids, (C) with laser delivery in OD eye and (D) without laser irradiation in OS eye. The laser dose was 1800 mJ/mm^2 (30 mW, 60 sec, 1 mm^2 area).

Scale: 50 μm. Apoptotic cells are marked as green dots. (E) Quantitative comparison of TUNEL +ve cells. N= 3 animals. Av± SD.